Acta Oncologica, 2014; 53: 1125–1134

informa
healthcare

ORIGINAL ARTICLE

Feasibility of experimental BT4C glioma models for somatostatin receptor 2-targeted therapies

AIDA KIVINIEMI[1,2], MARIA GARDBERG[3], ANU AUTIO[1], XIANG-GUO LI[1], VANINA D. HEUSER[3], HEIDI LILJENBÄCK[1,4], MEERI KÄKELÄ[1], HENRI SIPILÄ[1], JERE KURKIPURO[5,6], SEPPO YLÄ-HERTTUALA[5,6], JUHANI KNUUTI[1], HEIKKI MINN[7] & ANNE ROIVAINEN[1,4]

[1]*Turku PET Centre, Turku University Hospital and University of Turku, Turku, Finland,* [2]*Department of Radiology, Medical Imaging Centre of Southwest Finland, Turku University Hospital, Turku, Finland,* [3]*Department of Pathology, Turku University Hospital and University of Turku, Turku, Finland,* [4]*Turku Center for Disease Modeling, University of Turku, Turku, Finland,* [5]*AI Virtanen Institute, University of Eastern Finland, Kuopio, Finland,* [6]*Ark Therapeutics Oy, Kuopio, Finland and* [7]*Department of Oncology and Radiotherapy, Turku University Hospital, Turku, Finland*

ABSTRACT

Somatostatin receptor subtype 2 ($sstr_2$) is regarded as a potential target in malignant gliomas for new therapeutic approaches. Therefore, visualizing and quantifying tumor $sstr_2$ expression in vivo would be highly relevant for the future development of $sstr_2$-targeted therapies. The purpose of this study was to evaluate $sstr_2$ status in experimental BT4C malignant gliomas.

Methods. Rat BT4C malignant glioma cells were injected into BDIX rat brain or subcutaneously into nude mice. Tumor uptake of [^{68}Ga]DOTA-(Tyr^3)-Octreotide ([^{68}Ga]DOTATOC), a somatostatin analog binding to $sstr_2$, was studied by positron emission tomography/computed tomography (PET/CT). Additionally, subcutaneous tumor-bearing mice underwent PET imaging with 5-deoxy-5-[^{18}F]fluororibose-NOC ([^{18}F]FDR-NOC), a novel glycosylated peptide tracer also targeting $sstr_2$. Ex vivo tissue radioactivity measurements, autoradiography and immunohistochemistry were performed to study $sstr_2$ expression.

Results. Increased tumor uptake of [^{68}Ga]DOTATOC was detected at autoradiography with mean tumor-to-brain ratio of 68 ± 30 and tumor-to-muscle ratio of 9.2 ± 3.8 for rat glioma. High tumor-to-muscle ratios were also observed in subcutaneous tumor-bearing mice after injection with [^{68}Ga]DOTATOC and [^{18}F]FDR-NOC with both autoradiography (6.7 ± 1.5 and 4.3 ± 0.8, respectively) and tissue radioactivity measurements (6.5 ± 0.8 and 4.8 ± 0.6, respectively). Furthermore, $sstr_2$ immunohistochemistry showed positive staining in both tumor models. However, surprisingly low tumor signal compromised PET imaging. Mean SUV_{max} for rat gliomas was 0.64 ± 0.28 from 30 to 60 min after [^{68}Ga]DOTATOC injection. The majority of subcutaneous tumors were not visualized by [^{68}Ga]DOTATOC or [^{18}F]FDR-NOC PET.

Conclusions. Experimental BT4C gliomas show high expression of $sstr_2$. Weak signal in PET imaging, however, suggests only limited benefit of [^{68}Ga]DOTATOC or [^{18}F]FDR-NOC PET/CT in this tumor model for in vivo imaging of $sstr_2$ status.

Prognosis of glioblastoma, the most malignant glioma, remains poor [1]. Somatostatin receptor subtype 2 ($sstr_2$) has been studied as a promising target in malignant gliomas for new treatment strategies, such as transfer of genes to human glioblastoma cells via targeting adenoviral vectors to $sstr_2$ [2], or managing experimental gliomas with somatostatin analog that carries chemotherapeutic agent [3]. Preliminary clinical studies have also investigated $sstr_2$-targeted radionuclide therapy with yttrium-90-labeled 1,4,7,10-tetraazacyclododecane-1,4,7,10-tetraacetic acid-(Tyrosine^3)-Octreotide ([^{90}Y]

Correspondence: A. Roivainen, Turku PET Centre, Kiinamyllynkatu 4-8, 20521 Turku, Finland. Tel: +358 2 3132862. Fax: +358 2 2318191. E-mail: anne.roivainen@utu.fi

(Received 22 April 2014; accepted 9 May 2014)

ISSN 0284-186X print/ISSN 1651-226X online © 2014 Informa Healthcare
DOI: 10.3109/0284186X.2014.925577

DOTATOC) in human gliomas [4,5]. The therapeutic mechanism in all these new treatment strategies depends on $sstr_2$ expression, which is a prerequisite for a favorable effect. Therefore, a suitable experimental glioma model with established $sstr_2$ expression is warranted. Furthermore, recognizing the $sstr_2$ expression of the tumor in vivo before the potential therapy would be beneficial in order to optimize the treatment protocols [6]. In vivo PET imaging of gliomas with radioligands binding to $sstr_2$, such as Gallium-68-labeled DOTA-(Tyr^3)-Octreotide ([^{68}Ga]DOTATOC), however, has not been previously studied systematically for either experimental nor human gliomas.

[^{68}Ga]DOTATOC PET has been extensively studied with neuroendocrine tumors and more recently with meningeomas both of which express $sstr_2$ [7,8]. [^{68}Ga]DOTATOC demonstrates favorable pharmacokinetic properties with rapid binding to its G-protein coupled receptor as well as rapid clearance via the kidneys [7]. However, introduction of hydrophilic sugar moieties to the peptide tracer has shown to improve various properties of the tracer, such as enhanced penetration of the blood-brain barrier and increased tumor accumulation due to higher affinity [9]. Therefore, a new $sstr_2$ targeting glycosylated peptide tracer 5-deoxy-5-[Fluorine-18] fluororibose-1-NaI^3-octreotide ([^{18}F]FDR-NOC) was explored for the first time in preclinical practice [10].

The aim of this study was to evaluate experimental BT4C glioma models (orthotopic glioma in BDIX rats and subcutaneous tumors in nude mice) for expression of $sstr_2$ by means of immunohistochemistry, Western blot, uptake of [^{68}Ga]DOTATOC and [^{18}F]FDR-NOC by PET/CT in vivo, and by autoradiography and measurements of tissue radioactivity ex vivo. Additionally, [^{18}F]FDG PET/CT was performed to mice with subcutaneous tumors. To our knowledge, $sstr_2$ status and [^{68}Ga]DOTATOC uptake has not been previously studied in experimental glioma models. Furthermore, a novel glycosylated peptide tracer [^{18}F]FDR-NOC targeting $sstr_2$ is introduced.

Material and methods

Animal models

BT4C rat glioma cell line was originally derived from fetal BDIX rat brain cells, which were transferred to long-term culture after in vivo exposure to N-ethylnitrosurea [11]. Cells were grown in Dulbecco's modified Eagle medium (DMEM) supplemented with 10% fetal calf serum (Gibco, Paisley, Scotland), 2 mM glutamine, 2 mM sodium pyruvate and 50 µg/ml streptomycin at 37°C in the presence of 5% CO_2.

Male BDIX rats (Charles River, France) weighing 263–354 g (n = 9) were obtained for the stereotactic injections of BT4C glioma cells into the rat brain as described earlier [12]. Briefly, rats were anesthetized intraperitoneally (i.p.) with ketamine and medetomidine and placed into stereotactic apparatus (Kopf Instruments, Tujunga, CA, USA). A total of 10 000 BT4C cells in 5 µl of Optimem medium were slowly injected with a 25 µl Hamilton syringe 27 G needle (Hamilton, Bonaduz, Switzerland) into the right corpus callosum (coordinates: 1.0 mm caudal to bregma, 2.0 mm right to sutura sagittalis and depth of 2.5 mm). Needle was left in place for 5 min before removal to avoid backflow. The presence of rat BT4C orthotopic gliomas was verified by magnetic resonance imaging (MRI) 13 days after BT4C cell injection. Animals were kept under isoflurane anesthesia and MRI was performed using the 4.7 T magnet (Magnex, Abington, UK) interfaced to Varian Unity Inova (Palo Alto, CA, USA) console. T2-weighted spin-echo sequence (TR/TE = 2.5 s/0.08 s) was used. Image reconstruction was performed using MatLab 7.1. software (The MathWorks Inc., Natick, MA, USA).

To establish subcutaneous tumor model, male athymic nude mice (Harlan) were kept under isoflurane anesthesia (induction 3–4% and maintenance 2–3%) while 250 000 BT4C cells in 100 µl of Matrigel (Matrigel Matrix, BD Biosciences) were injected subcutaneously into the neck and left limb of each mouse (n = 16).

All animal care and experiments were approved by the national Animal Experiment Board in Finland (21.12.2011 PH1296A) and carried out in compliance with Finnish laws relating to the conduct of animal experimentation.

Preparation of [^{68}Ga]DOTATOC, [^{18}F]FDR-NOC and [^{18}F]FDG

The radiochemical purity of [^{68}Ga]DOTATOC exceeded 99% and the specific radioactivity was 7–26 GBq/µmol. [^{18}F]FDR-NOC was prepared as previously described [10,13] resulting in radiochemical purity of 99% and specific radioactivity of 33 GBq/µmol. Synthesis of [^{18}F]FDG and more detailed description on the preparation of [^{68}Ga]DOTATOC and [^{18}F]FDR-NOC is presented in the Appendix (available online at: http://informahealthcare.com/doi/abs/10.3109/0284186X.2014.925577).

[^{68}Ga]DOTATOC, [^{18}F]FDR-NOC and [^{18}F]FDG PET/CT imaging

PET/CT was performed 23–25 days after stereotactic BT4C injection into BDIX rat brain or 26–30

days after subcutaneous BT4C injection with a dedicated small animal PET/CT scanner with an axial FOV of 12.5 cm (Inveon Multimodality PET/CT, Siemens Medical Solutions, Knoxville, TN, USA). [^{68}Ga]DOTATOC PET/CT was performed to nine BDIX rats and eight subcutaneous tumor-bearing mice. Eight additional mice with subcutaneous tumors underwent [^{18}F]FDR-NOC PET/CT. On the previous day these animals were imaged with [^{18}F]FDG PET/CT. PET/CT imaging was accomplished also for rats demonstrating no tumor in MRI (n = 2). Animals were anesthetized with isoflurane (induction 4% and maintenance 1.5–2%) and were kept on a warm pallet during the imaging procedure. One rat or two mice at a time were imaged. Following CT scan for attenuation correction, animals were intravenously (i.v.) injected with [^{68}Ga]DOTATOC (rats 30.8 ± 3.2 MBq; mice 11.6 ± 2.1 MBq) or [^{18}F]FDR-NOC (13.5 ± 1.1 MBq). Dynamic imaging lasting for 60 min started at the time of injection. Static [^{18}F]FDG PET/CT for 20 min started 45 min after injection with mean injected dose 14.5 ± 0.4 MBq.

PET data acquired in list mode were iteratively reconstructed with a two-dimensional (2D) ordered subsets expectation maximization algorithm (OSEM2D) with 4 iterations and 16 subsets into 12 × 5 s, 12 × 30 s, 8 × 60 s, 3 × 300 s and 3 × 600 s frames. A reconstructed image had 38 frames and 128 × 128 × 159 matrix size with a voxel size of 0.776 × 0.776 × 0.796 mm.

Quantitative analysis was performed by defining spherical volumes of interest (VOI) on the tumor, normal brain, heart, liver and kidney. Brain tumor was localized next to the cranial drill hole. Time-activity curves (TACs) were extracted from the corresponding dynamic images (Carimas 2.8; Turku PET Centre, Turku, Finland; http://www.turkupetcentre.fi/carimas). The average radioactivity concentration in the VOI (kBq/mL) was used for further analyses. The uptake was reported as standardized uptake value (SUV), which was calculated as a ratio of radioactivity of the VOI and injected radioactivity (kBq) divided by body weight (g). The radioactivity remaining in the tail was compensated.

Tumor uptake in [^{18}F]FDG PET/CT was reported as scaled SUV that takes into consideration the blood glucose levels measured before and after the scanning. Scaled SUV is calculated as the mean SUV multiplied by blood glucose level of individual animal divided by mean blood glucose level of all the animals.

Dynamic PET data from BDIX rats was used for [^{68}Ga]DOTATOC tracer kinetic modeling. Logan plots for rat BT4C orthotopic gliomas with muscle as a reference tissue were applied to attain distribution volume ratio (DVR). We used 10 min as the starting point for the linear regression. Binding potential (BP) corresponds to the density of available receptors and is calculated as BP = DVR − 1. Muscle was selected as a reference tissue due to its low sstr$_2$ expression.

Tissue radioactivity measurements and stability of [^{68}Ga]DOTATOC and [^{18}F]FDR-NOC

Animals were killed immediately after [^{68}Ga]DOTATOC or [^{18}F]FDR-NOC PET/CT imaging. Samples of different tissues, blood, plasma and urine were obtained and radioactivity was measured with a well-type gamma counter (Triathler Gamma with external 3" NaI detector, Hidex Oy, Turku, Finland), cross-calibrated with a dose calibrator and PET/CT camera. Plasma was separated by centrifugation (2000 × *g* for 5 min at 4°C).

The in vivo stability of [^{68}Ga]DOTATOC and [^{18}F]FDR-NOC at 60 min post-injection was tested by radio-HPLC analysis as described in Supplementary Appendix, available online at: http://informahealthcare.com/doi/abs/10.3109/0284186X.2014.925577. The percentage of intact tracer was calculated from chromatograms based on the peak areas of different radioactive species.

Autoradiography analysis

Tumor, brain and muscle uptake of [^{68}Ga]DOTATOC and [^{18}F]FDR-NOC were studied with digital autoradiography. Tissues were dissected immediately after PET/CT imaging, frozen in dry ice and sectioned with cryomicrotome into serial 8- and 20-μm sections at -15°C. Tissue sections were then thaw-mounted onto microscope slides and opposed to an imaging plate (Fuji Imaging Plate BAS-TR 2025, Fuji Photo Film Co., Ltd., Tokyo, Japan). After an exposure time of 2.5 h for [^{68}Ga]DOTATOC and 4 h for [^{18}F]FDR-NOC, the imaging plates were scanned with the Fuji Analyzer BAS-5000 (Fuji Photo Film Co., Ltd., Tokyo, Japan; internal resolution of 25 μm).

Images of tumor, brain and muscle sections were analyzed for count densities (photostimulated luminescence units [PSL]/mm^2) with an image-analysis program (Tina 2.1, Raytest Isotopenmessgeräte GmbH, Straubenhardt, Germany). Circular ROIs were defined for the tumor in accordance with hematoxylin and eosin staining from areas of highest tumor cellularity. The background count densities were subtracted from the image data. Several tissue sections were analyzed for each animal and results are expressed as mean values (± SD).

Sstr$_2$ immunohistochemistry and Western blot analysis

Hematoxylin and eosin (H&E) staining and sstr$_2$ immunohistochemistry were performed on 8 μm

slides adjacent to the 20 μm slides used for autoradiography analysis. The $sstr_2$ monoclonal antibody UMB-1 (Abcam, Cambridge, UK) has previously been extensively characterized [14,15]. Endothelial cells known to express $sstr_2$ functioned as positive internal control and brain white matter and muscle as negative control [16]. Additional immunohistochemical stainings (CD34 and CD68) and Supplementary Table I (available online at: http://informahealthcare.com/doi/abs/10.3109/0284186X.2014.925577)with details of the conditions used for the immunohistochemistry are presented in the Appendix.

$Sstr_2$ expression in BT4C cell line was further studied in vitro using Western blot analysis (detailed protocol in the Appendix). Tissue samples from rat adrenal gland, kidney, and spleen known to express $sstr_2$ served as positive controls [17].

Statistical analyses

Data are presented as mean ± SD. Normality was tested with Shapiro-Wilk test. Statistical dependence between BP and SUV was calculated with Spearman's rank correlation. Independent t-test was used for parametric variables and independent-samples Mann-Whitney U-test was applied for non-parametric variables to compare the uptake between the tumor and reference tissues, and the uptake between [^{68}Ga]DOTATOC and [^{18}F]FDR-NOC in biodistribution data. p-Values were calculated using two-tailed test and less than 0.05 was considered statistically significant. Statistical analyses were conducted using SPSS 17 for Mac (SPSS, Inc., Chicago, IL, USA).

Results

Animal model and BT4C glioma histology

BT4C glioma cell injection induced intracranial tumor in seven BDIX rats of nine as confirmed by MRI 13 days after injection. The H&E staining demonstrated tumors with high cellularity, small necrotic areas and an infiltrative border. Neoplastic cells displayed marked pleomorphism and nuclear atypia. Mitotic figures were frequent and neovascularization was also detected. Histologically, rat orthotopic BT4C glioma was highly similar to human glioblastoma. Mean tumor dimensions were 4.2×3.0 mm. Subcutaneous BT4C tumors were induced successfully in all nude mice reaching an average size of 5.4×4.7 mm. Histologically they resembled orthotopic BT4C glioma, however, with less neovascularization and necrotic areas. In addition, subcutaneous BT4C tumors presented diffuse leukocytosis and areas of edematous subcutaneous fat tissue.

PET/CT imaging of tumor

Visualization of BT4C tumors with [^{68}Ga]DOTATOC or [^{18}F]FDR-NOC PET/CT imaging was limited (Figure 1). Rat orthotopic BT4C gliomas were all modestly visualized with [^{68}Ga]DOTATOC PET ($n = 6$, one PET/CT imaging of a rat bearing a tumor failed). However, of sixteen subcutaneous BT4C tumors in nude mice only six were visualized with [^{68}Ga]DOTATOC PET and only three were visualized with [^{18}F]FDR-NOC PET. Mean SUV_{max} values (± SD) obtained from PET data from 30 to 60 min after injection was 0.64 ± 0.28 for orthotopic glioma with [^{68}Ga]DOTATOC, 0.40 ± 0.11 for subcutaneous tumor with [^{68}Ga]DOTATOC, and 0.53 ± 0.07 for subcutaneous tumor with [^{18}F]FDR-NOC. In rat orthotopic glioma, a mean SUV_{max} ratio between the tumor and contralateral normal brain was 2.0 ± 0.6 from 30 to 60 min after injection. In addition, [^{18}F]FDG PET/CT was performed to eight nude mice bearing subcutaneous BT4C tumors to study their metabolic activity. [^{18}F]FDG uptake was increased in all subcutaneous tumors with mean scaled SUV_{max} of 1.4 ± 0.7.

The calculated BP for [^{68}Ga]DOTATOC in the rat orthotopic BT4C gliomas using muscle as a reference tissue was 0.76 ± 0.39 ($n = 5$). Logan plot from one rat was excluded from the analysis due to low R-squared value of 47%. For other plots, mean R-squared value was 99.8% meaning good fitting of the data to the kinetic model used. No correlation, however, was found between BP and SUV_{max} values obtained from PET data from 30 to 60 min after injection.

Tissue radioactivity measurements and stability of [^{68}Ga]DOTATOC and [^{18}F]FDR-NOC

Ex vivo biodistribution data from tissue radioactivity measurements at 60 min after injection is presented in Table I. Subcutaneous BT4C tumors in mice showed high uptake of both [^{68}Ga]DOTATOC and [^{18}F]FDR-NOC when compared to the reference tissue muscle ($p \leq 0.001$ for both tracers). Between the two tracers, tumor uptake was higher with [^{18}F]FDR-NOC ($p = 0.021$). However, due to increased radioactivity concentration also in reference tissues, the tumor-to-muscle and tumor-to-brain ratios were actually diminished with [^{18}F]FDR-NOC compared to [^{68}Ga]DOTATOC. Rat orthotopic BT4C gliomas were not analyzed with a gamma counter in order to obtain intact brain tumor for autoradiography analysis.

Tissue radioactivity measurements after [^{68}Ga]DOTATOC injection showed high values in the kidneys and urine and low values in other non-target

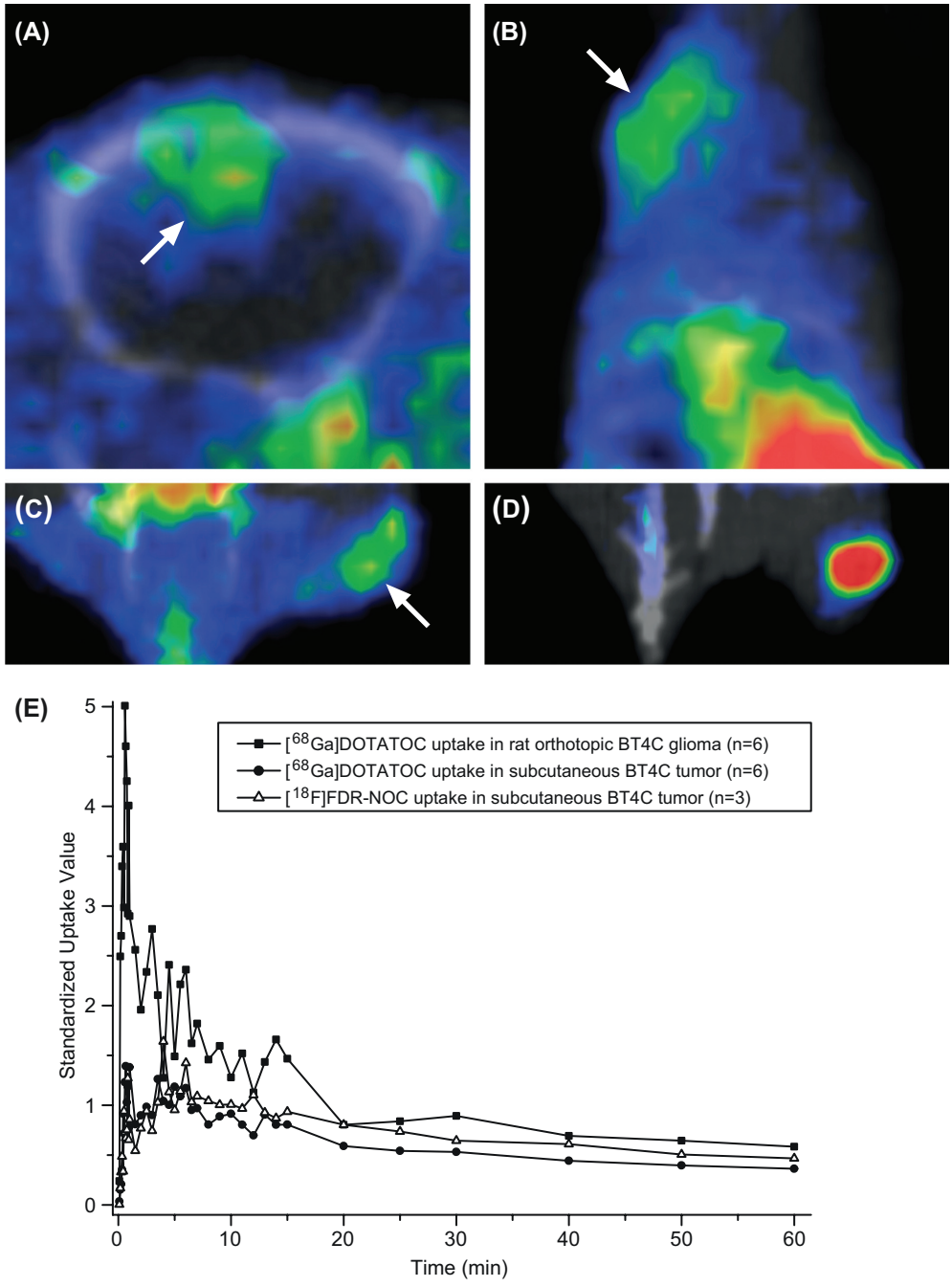

Figure 1. Visualization of BT4C tumors was suboptimal with [^{68}Ga]DOTATOC and [^{18}F]FDR-NOC PET/CT. Representative (A) axial PET/CT image of a BDIX rat brain with an orthotopic BT4C glioma and (B) coronal PET/CT image of a mouse bearing a subcutaneous BT4C tumor in the neck after [^{68}Ga]DOTATOC injection i.v. (C,D) Representative coronal PET/CT images of the same mouse bearing a subcutaneous tumor in the left limb after [^{18}F]FDR-NOC (C) and [^{18}F]FDG (D) injections i.v. The tumor is clearly visualized with [^{18}F]FDG PET/CT. Tumors are indicated with an arrow. PET images represent mean radioactivity concentration at 30–60 min after tracer injection. (E) Time-activity curves of BT4C tumors after injection with [^{68}Ga]DOTATOC or [^{18}F]FDR-NOC. Uptake values are presented as mean SUV_{max}.

organs (Table I). Rapid clearance from blood and renal excretion was also confirmed by [^{68}Ga]DOTATOC uptake data obtained from 60 min dynamic PET imaging in mice (Figure 2). [^{18}F]FDR-NOC, however, in addition to elimination via kidneys was also eliminated via hepatobiliary pathway as indicated by significantly increased radioactivity in the liver and small intestine compared to [^{68}Ga]DOTATOC ($p \leq 0.001$).

In vivo stability of [^{68}Ga]DOTATOC in plasma of BDIX rats and nude mice at 60 min after injection was excellent; the percentage of intact

Table I. Tissue radioactivity measurements at 60 minutes after injection with [^{68}Ga]DOTATOC and [^{18}F]FDR-NOC.

	Rat orthotopic BT4C glioma [^{68}Ga]DOTATOC n = 9	Mice subcutaneous BT4C tumor		
		[^{68}Ga]DOTATOC n = 8	[^{18}F]FDR-NOC n = 8	p
Tumor	NA	0.31 ± 0.11	0.38 ± 0.04	*
Muscle	0.10 ± 0.04	0.05 ± 0.02	0.08 ± 0.01	*
Brain	NA	0.02 ± 0.02	0.03 ± 0.00	*
Heart	0.24 ± 0.06	0.10 ± 0.04	0.27 ± 0.04	**
Lung	0.70 ± 0.14	0.34 ± 0.09	0.81 ± 0.07	**
Liver	0.47 ± 0.40	0.12 ± 0.03	4.54 ± 0.34	**
Pancreas	NA	0.63 ± 0.23	0.68 ± 0.23	
Spleen	0.56 ± 0.57	0.10 ± 0.03	0.25 ± 0.04	**
Small intestine	0.60 ± 0.20	0.18 ± 0.05	1.42 ± 0.69	**
Kidney	9.21 ± 4.87	2.73 ± 1.16	2.68 ± 0.29	
Skin	0.33 ± 0.09	0.31 ± 0.11	0.41 ± 0.05	*
Blood	0.65 ± 0.16	0.28 ± 0.12	0.71 ± 0.10	**
Plasma	1.12 ± 0.25	0.25 ± 0.10	0.66 ± 0.11	**
Urine	113 ± 55.3	41.0 ± 15.8	26.5 ± 12.3	
Tumor-to-muscle ratio	NA	6.46 ± 0.77	4.79 ± 0.64	*
Tumor-to-brain ratio	NA	22.3 ± 9.08	15.1 ± 1.91	*

Results are expressed as SUVs (mean ± SD). NA = not analyzed. *$p < 0.05$; **$p \leq 0.001$ between [^{68}Ga]DOTATOC and [^{18}F]FDR-NOC in nude mice bearing subcutaneous BT4C tumors.

[^{68}Ga]DOTATOC was 99–100%. Also [^{18}F]FDR-NOC showed high in vivo stability with 94–96% of intact tracer in plasma at 60 min after injection. Major radioactive metabolite in plasma was present at retention time 4.85 min. Intact [^{18}F]FDR-NOC detected in urine 60 min after injection varied from 10% to 81%.

Autoradiography

The autoradiography analysis (Table II) showed a significant uptake of [^{68}Ga]DOTATOC in the rat orthotopic BT4C glioma when compared to contralateral normal brain ($p = 0.002$) or muscle ($p = 0.002$) with mean tumor-to-brain ratio of 68.1 ± 30.4 and tumor-to-muscle ratio of 9.2 ± 3.8. Also subcutaneous BT4C tumors presented in autoradiography high uptake of both [^{68}Ga]DOTATOC and [^{18}F]FDR-NOC compared to muscle ($p < 0.001$ for both) with tumor-to-muscle ratio of 6.7 ± 1.5 and 4.3 ± 0.8, respectively. Uptake of [^{68}Ga]DOTATOC within the orthotopic BT4C glioma was mainly uniform as demonstrated in Figure 3. Slightly higher uptake was observed in subcutaneous BT4C tumors in areas of edematous fat tissue. These areas, however, were disregarded from analysis.

Immunohistochemistry and Western blot analysis

Immunohistochemical staining of $sstr_2$ was distinctly positive in rat orthotopic BT4C glioma (Supplementary Figure 1, available online at: http://informahealthcare.com/doi/abs/10.3109/0284186X.2014.925577). Receptors were homogenously distributed in rat glioma with positive staining in more than 95% of the neoplastic cells. Subcutaneous BT4C tumors in nude mice showed more heterogeneous $sstr_2$ immunostaining compared to orthotopic gliomas with positive staining in 40–80% of the neoplastic cells. The staining pattern was mainly intracellular but also membranous staining was detected. Results of CD34 and CD68 immunostaining are presented in the Appendix.

Western blot analysis demonstrated $sstr_2$ expression of BT4C glioma cells by giving two major bands at ~30–32 kDa near to the expected $sstr_2$ molecular size. Same major bands were also detected in rat control tissues (Supplementary Figure 2, available online at: http://informahealthcare.com/doi/abs/10.3109/0284186X.2014.925577).

Discussion

Suitable experimental glioma model expressing $sstr_2$ is warranted as the implications for $sstr_2$-targeted therapies in gliomas continue to expand. In addition, detecting $sstr_2$ in vivo by PET imaging would be highly beneficial for the planning of therapies targeting $sstr_2$ and in the follow-up of these strategies. In this study, we validated the $sstr_2$ status of two BT4C glioma models with PET/CT imaging, autoradiography, tissue radioactivity measurements,

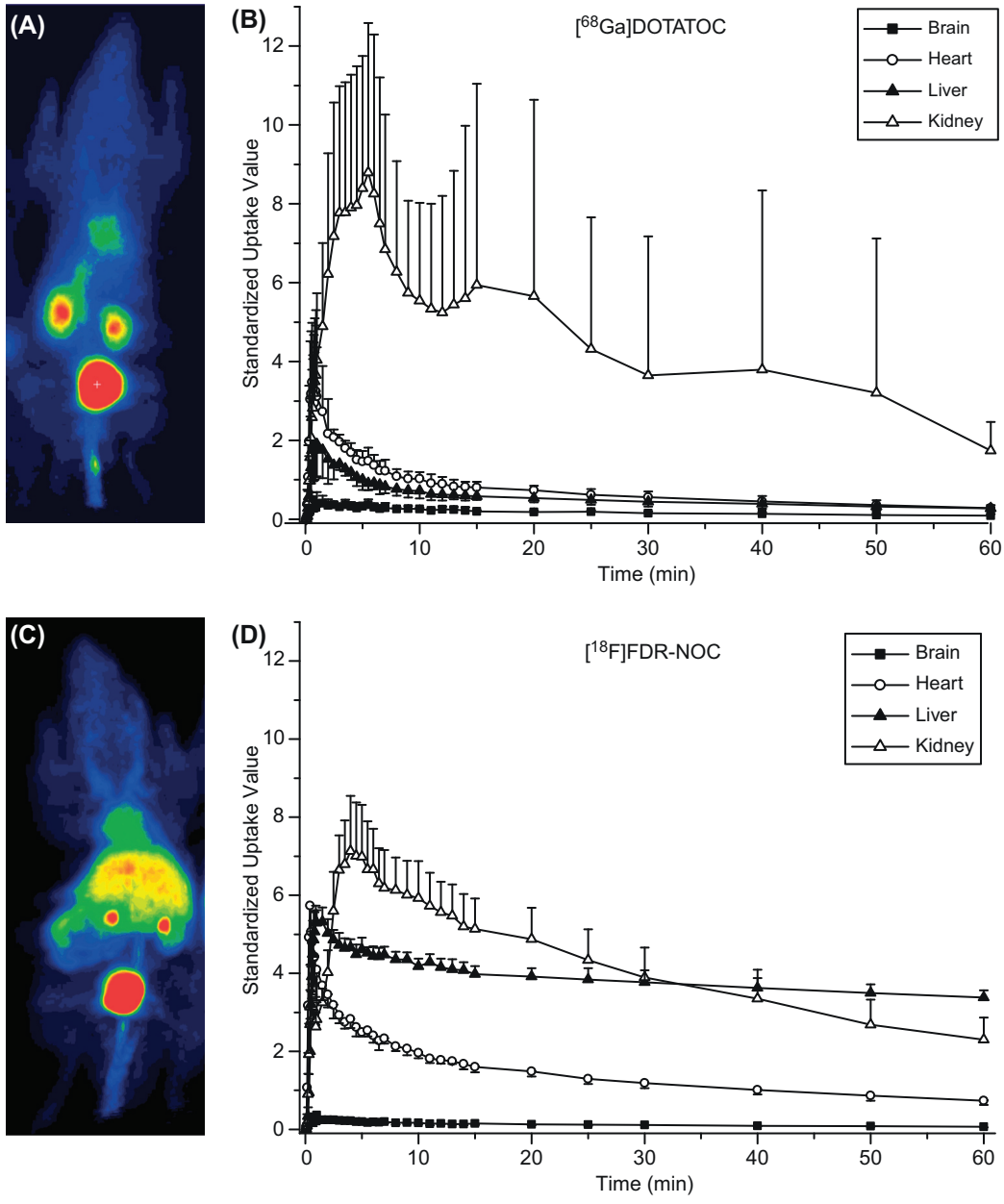

Figure 2. [^{18}F]FDR-NOC is rapidly excreted via hepatobiliary and urinary pathways. Representative whole-body coronal PET images of mice i.v. injected with (A) [^{68}Ga]DOTATOC or (C) [^{18}F]FDR-NOC and (B, D) corresponding time-activity curves for brain, heart, liver and kidney. Increased liver uptake of [^{18}F]FDR-NOC can be clearly seen. Uptake values are presented as SUV_{mean} ($\pm$ SD) of all mice. Dynamic PET images are averaged from 0 to 60 min after injection.

immunohistochemistry, and Western blotting of the BT4C tumor cells. We found high tumor-to-muscle ratios in autoradiography and tissue radioactivity measurements ex vivo after injections with [^{68}Ga]DOTATOC and [^{18}F]FDR-NOC, both of which are somatostatin analogs binding to $sstr_2$. Positive staining for $sstr_2$ in immunohistochemistry and Western blotting of BT4C cells supported the findings. Despite the positive ex vivo results, however, [^{68}Ga]DOTATOC and [^{18}F]FDR-NOC performed rather poorly in PET imaging in vivo.

Our autoradiography analysis demonstrated a 68-fold higher uptake of [^{68}Ga]DOTATOC in rat orthotopic BT4C glioma compared to contralateral normal brain. DOTATOC binds predominantly to $sstr_2$ thus verifying 'functional' $sstr_2$ in BT4C tumors. In line with this, $sstr_2$ expression was also immunohistochemically observed in majority (95%) of rat BT4C glioma cells. The binding potential for [^{68}Ga]DOTATOC in rat gliomas (0.76 ± 0.39) was positive though remained at a low level. It must thus be speculated that [^{68}Ga]DOTATOC tumor accumulation,

Table II. Autoradiography results of tissue uptake of [^{68}Ga]DOTATOC and [^{18}F]FDR-NOC.

	Rat orthotopic BT4C glioma [^{68}Ga]DOTATOC n = 7	Mice subcutaneous BT4C tumor		
		[^{68}Ga]DOTATOC n = 8	[^{18}F]FDR-NOC n = 8	P
Tumor	9.8 ± 1.8	17.4 ± 7.5	75 ± 18	**
Muscle	1.2 ± 0.4	2.7 ± 1.6	18 ± 3.1	**
Brain	0.2 ± 0.1	ND	3.3 ± 1.2	
Tumor-to-muscle ratio	9.2 ± 3.8	6.7 ± 1.5	4.3 ± 0.8	**
Tumor-to-brain ratio	68 ± 30	ND	25 ± 9.2	

Results are expressed as PSL/mm^2 (mean ± SD). ND = not detectable, the brain could not be distinguished from the background. **$p \leq 0.001$ between [^{68}Ga]DOTATOC and [^{18}F]FDR-NOC in nude mice bearing subcutaneous BT4C tumors.

in addition to active receptor binding, may also be passive due to a defective blood-brain barrier. Disruption of blood-brain barrier is manifested also in rat BT4C glioma as indicated by MRI contrast enhancement [18]. The relationship between blood-brain barrier integrity and uptake of [^{68}Ga]DOTATOC is important for further validation of sstr$_2$-targeted therapy in glioma and is in the focus of our ongoing study.

Rat BT4C orthotopic gliomas were all visualized in PET/CT with mean SUV_{max} 0.64 ± 0.28 from 30 to 60 min from injection with [^{68}Ga]DOTATOC. However, most subcutaneous BT4C tumors could not be visualized with [^{68}Ga]DOTATOC PET/CT possibly relating to less intensive immunohistochemical sstr$_2$ staining in subcutaneous tumors. Consequently, we wanted to study whether glycosylation of the tracer peptide would improve tumor uptake and induce sufficient signal intensity for PET imaging. It has been well documented that sugar conjugation is a powerful method to improve tracer pharmacokinetics [9,19]. Schottelius et al. studied the pharmacokinetics of a sstr$_2$ agonist conjugated with different carbohydrates, such as glucose and maltose, and found elevated tumor uptake with excellent tumor-to-organ ratios [9]. Using [^{18}F]FDR as a prosthetic group for labeling peptides is a novel method for glycosylating peptides for PET [10,13]. Indeed, significant increase in [^{18}F]FDR-NOC uptake was detected in subcutaneous BT4C tumors compared to [^{68}Ga]DOTATOC with both methods of autoradiography and tissue radioactivity measurements. Visualization of the subcutaneous tumors with [^{18}F]FDR-NOC PET/CT, however, was not

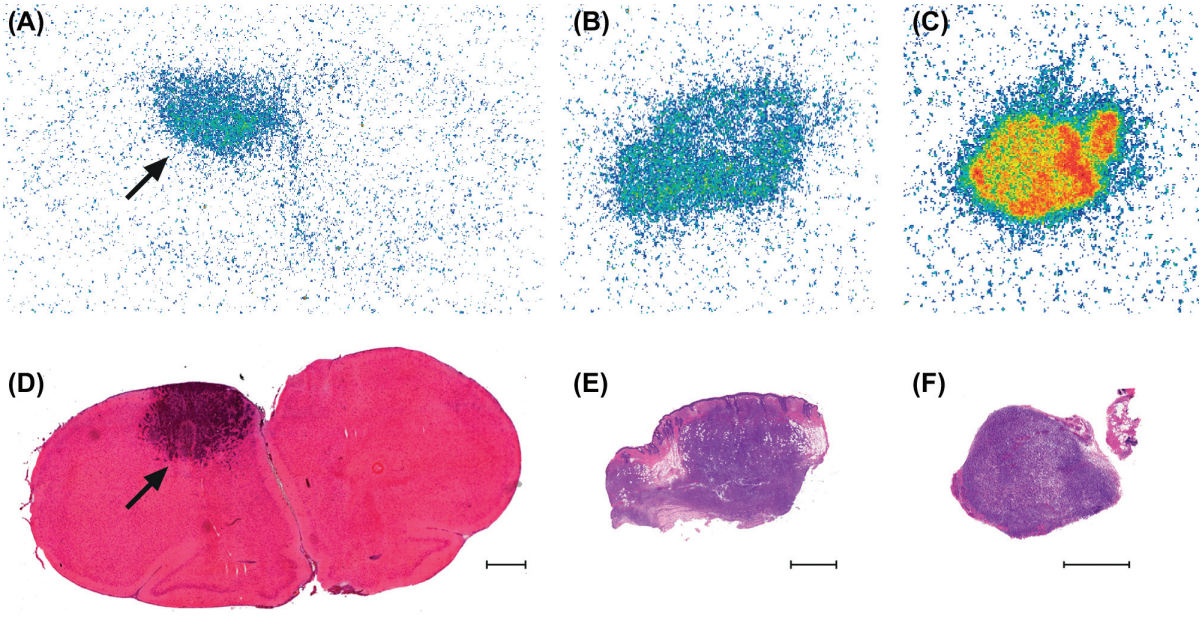

Figure 3. Autoradiography demonstrates high tumor uptake of [^{68}Ga]DOTATOC and [^{18}F]FDR-NOC. Representative autoradiographs showing (A) uptake of [^{68}Ga]DOTATOC in rat orthotopic BT4C glioma, (C) uptake of [^{68}Ga]DOTATOC in subcutaneous BT4C tumor, and (E) uptake of [^{18}F]FDR-NOC in another subcutaneous BT4C tumor. (B, D, F) Lower panel shows H&E stainings of the corresponding sections. Arrow indicates the tumor in rat brain. Bar = 1 mm.

improved compared to [^{68}Ga]DOTATOC PET/CT. Although autoradiography is known to have higher sensitivity compared to PET especially with small target lesions [20,21], the rate of discrepancy between PET and ex vivo studies was surprising. It can be speculated that ^{68}Ga-radionuclide may not be optimal for imaging small target lesions due to its high positron energy and corresponding large positron range in tissue. ^{18}F-radionuclide possesses lower positron energy and may thus be more convenient for imaging small objects with PET. However, [^{18}F]FDR-NOC was rapidly excreted via the kidneys and hepatobiliary pathway, which may have downgraded appropriate tissue binding.

Uptake in liver and small intestine was significantly increased 60 min after injection with [^{18}F]FDR-NOC compared to [^{68}Ga]DOTATOC as presented in Table I. Time-activity curves from dynamic PET data show that liver uptake of [^{18}F]FDR-NOC was elevated already during the first minutes after injection and remained high for the whole 60 minutes suggesting rapid excretion via hepatobiliary pathway (Figure 2). In addition, [^{18}F]FDR-NOC was eliminated through the kidneys with an extent similar to [^{68}Ga]DOTATOC. This did not correspond to earlier studies where glycosylation of the tracer peptides improved pharmacokinetics due to increased hydrophilicity of the tracer leading to favored excretion pathway via kidneys and reduction in liver uptake [9,19]. Our opposite finding of increased liver uptake with glycosylated [^{18}F]FDR-NOC compared to [^{68}Ga]DOTATOC, however, may be related to the disadvantageous comparison for [^{18}F]FDR-NOC, since [^{68}Ga]DOTATOC already possesses highly favorable pharmacokinetics.

[^{18}F]FDR-NOC uptake was significantly higher in almost all non-target organs, including brain, when compared to [^{68}Ga]DOTATOC uptake in mice bearing subcutaneous tumors (Table I). This may be due to improved biological properties of the glycosylated tracer, such as bioavailability or penetration of the BBB as discussed earlier. Secondly, tracer peptides TOC and NOC have different affinity profiles for somatostatin receptor subtypes. While both peptides have high affinity for sstr$_2$, NOC demonstrates stronger binding also to somatostatin receptor subtypes 3 and 5 (sstr$_3$ and sstr$_5$) [22]. Sstr$_2$ is known to be the most abundant subtype in most tumor types. However, the effect of sstr$_3$ and sstr$_5$ expression to [^{18}F]FDR-NOC uptake cannot be excluded since their expression was not analyzed in this study.

Sstr$_2$ immunostaining with UMB-1 antibody detected sstr$_2$ protein expression throughout the rat orthotopic BT4C glioma in almost all tumor cells. Staining pattern in subcutaneous BT4C tumors was more heterogeneous with areas of negative staining as well. UMB-1 is a monoclonal antibody that has been thoroughly studied in recent years and is considered to be the best available tool for semiquantitative characterization of tumor sstr$_2$ expression [15]. In addition, reliability of UMB-1 staining was warranted in our study with both positive and negative internal controls. The subcellular localization of sstr$_2$ immunoreactivity was mainly cytoplasmic in both orthotopic and subcutaneous BT4C tumors. This corresponds well to a previous in vivo study where internalization of sstr$_2$ in rat AR42J tumor cells was seen already 2.5 min after i.v. injection of sstr$_2$ agonist and was still detectable at 6 h after injection [14]. Sstr$_2$ receptor internalization and subsequent accumulation into the tumor cells is important especially considering the efficacy of targeted radiotherapy with somatostatin analogs, such as [^{90}Y]DOTATOC.

[^{68}Ga]DOTATOC PET/CT is in clinical use for staging and follow-up of neuroendocrine tumors. It is also used to evaluate the suitability of the tumor for in vivo sstr$_2$ targeting radiotherapy since neuroendocrine tumors have shown good correlation between sstr$_2$ immunostaining and increased uptake of [^{68}Ga]DOTATOC in PET/CT imaging [23]. Körner et al., studied immunohistochemistry of neuroendocrine tumors with UMB-1, the same antibody used in our study, and correlated it to the actual receptor levels detected by autoradiography [15]. They found that intensive UMB-1 staining in more than 10% of tumor cells predicted high autoradiographic receptor levels, which is a prerequisite for therapeutic sstr$_2$ targeting. In our study, especially rat orthotopic BT4C gliomas showed very intensive positive staining with UMB-1 antibody in more than 95% of the glioma cells suggesting a potential role for this experimental model in sstr$_2$-targeted therapies.

We have validated sstr$_2$ status of two BT4C glioma models and conclude that these tumors express sstr$_2$ as demonstrated with autoradiography, tissue radioactivity measurements, immunohistochemistry, and Western blotting. Especially rat orthotopic BT4C glioma is warranted to be further evaluated in treatments attempting to target sstr$_2$ in malignant glioma. Unfortunately, follow-up using [^{68}Ga]DOTATOC or [^{18}F]FDR-NOC PET/CT imaging was suboptimal due to low tumor signal.

Acknowledgments

We thank Helena Ahtinen (Turku PET Centre, Turku University Hospital), Erica Nyman and Marja-Riitta Kajaala (Turku Centre for Disease Modeling, University of Turku), Marko Tirri (Department of Physiology, University of Turku), Minnamaija

Lintunen, Sinikka Kollanus and Jaakko Liippo (Department of Pathology, Turku University Hospital) for excellent technical assistance.

Declaration of interest: The authors report no conflicts of interest. The authors alone are responsible for the content and writing of the paper.

This study was conducted within the Finnish Centre of Excellence in Cardiovascular and Metabolic Diseases supported by the Academy of Finland, University of Turku, Turku University Hospital, and Åbo Akademi University. In addition, the study was financially supported by a grant from the Foundation for the Finnish Cancer Organisations. Aida Kiviniemi is a Ph.D. student supported by the National Graduate School of Clinical Investigation.

References

[1] Ohgaki H. Epidemiology of brain tumors. Methods Mol Biol 2009;472:323–42.

[2] Lecolle K, Begard S, Caillierez R, Demeyer D, Grellier E, Loyens A, et al. Sstr2A: A relevant target for the delivery of genes into human glioblastoma cells using fiber-modified adenoviral vectors. Gene Ther 2013;20:283–97.

[3] Pozsgai E, Schally AV, Halmos G, Rick F, Bellyei S. The inhibitory effect of a novel cytotoxic somatostatin analogue AN-162 on experimental glioblastoma. Horm Metab Res 2010;42:781–6.

[4] Schumacher T, Hofer S, Eichhorn K, Wasner M, Zimmerer S, Freitag P, et al. Local injection of the ^{90}Y-labelled peptidic vector DOTATOC to control gliomas of WHO grades II and III: An extended pilot study. Eur J Nucl Med Mol Imaging 2002;29:486–93.

[5] Heute D, Kostron H, von Guggenberg E, Ingorokva S, Gabriel M, Dobrozemsky G, et al. Response of recurrent high-grade glioma to treatment with ^{90}Y-DOTATOC. J Nucl Med 2010;51:397–400.

[6] Malinen E, Muren LP. Image guided therapy – Do we get the picture? Acta Oncol 2014;53:3–5.

[7] Breeman WA, de Blois E, Sze Chan H, Konijnenberg M, Kwekkeboom DJ, Krenning EP. ^{68}Ga-labeled DOTA-peptides and ^{68}Ga-labeled radiopharmaceuticals for positron emission tomography: Current status of research, clinical applications, and future perspectives. Semin Nucl Med 2011;41:314–21.

[8] Combs SE, Welzel T, Habermehl D, Rieken S, Dittmar JO, Kessel K, et al. Prospective evaluation of early treatment outcome in patients with meningiomas treated with particle therapy based on target volume definition with MRI and ^{68}Ga-DOTATOC-PET. Acta Oncol 2013;52: 514–20.

[9] Schottelius M, Wester HJ, Reubi JC, Senekowitsch-Schmidtke R, Schwaiger M. Improvement of pharmacokinetics of radioiodinated Tyr(3)-octreotide by conjugation with carbohydrates. Bioconjug Chem 2002;13:1021–30.

[10] Li XG, Helariutta K, Roivainen A, Jalkanen S, Knuuti J, Airaksinen AJ. Using 5-deoxy-5-[^{18}F]fluororibose to glycosylate peptides for positron emission tomography. Nat Protoc 2014;9:138–45.

[11] Laerum OD, Rajewsky MF. Neoplastic transformation of fetal rat brain cells in culture after exposure to ethylnitrosourea in vivo. J Natl Cancer Inst 1975;55:1177–87.

[12] Tyynelä, Sandmair A, Turunen M, Vanninen R, Vainio P, Kauppinen R, et al. Adenovirus-mediated herpes simplex virus thymidine kinase gene therapy in BT4C rat glioma model. Cancer Gene Ther 2002;9:917–24.

[13] Li XG, Autio A, Ahtinen H, Helariutta K, Liljenbäck H, Jalkanen S, et al. Translating the concept of peptide labeling with 5-deoxy-5-[^{18}F]fluororibose into preclinical practice: ^{18}F-labeling of Siglec-9 peptide for PET imaging of inflammation. Chem Commun (Camb) 2013;49:3682–4.

[14] Waser B, Tamma ML, Cescato R, Maecke HR, Reubi JC. Highly efficient in vivo agonist-induced internalization of sst2 receptors in somatostatin target tissues. J Nucl Med 2009;50:936–41.

[15] Korner M, Waser B, Schonbrunn A, Perren A, Reubi JC. Somatostatin receptor subtype 2A immunohistochemistry using a new monoclonal antibody selects tumors suitable for in vivo somatostatin receptor targeting. Am J Surg Pathol 2012;36:242–52.

[16] Watson JC, Balster DA, Gebhardt BM, O'Dorisio TM, O'Dorisio MS, Espenan GD, et al. Growing vascular endothelial cells express somatostatin subtype 2 receptors. Br J Cancer 2001;85:266–72.

[17] Patel YC, Greenwood MT, Panetta R, Demchyshyn L, Niznik H, Srikant CB. The somatostatin receptor family. Life Sci 1995;57:1249–65.

[18] Thorsen F, Ersland L, Nordli H, Enger PO, Huszthy PC, Lundervold A, et al. Imaging of experimental rat gliomas using a clinical MR scanner. J Neurooncol 2003;63:225–31.

[19] Haubner R, Wester HJ, Burkhart F, Senekowitsch-Schmidtke R, Weber W, Goodman SL, et al. Glycosylated RGD-containing peptides: Tracer for tumor targeting and angiogenesis imaging with improved biokinetics. J Nucl Med 2001;42:326–36.

[20] Schmidt KC, Smith CB. Resolution, sensitivity and precision with autoradiography and small animal positron emission tomography: Implications for functional brain imaging in animal research. Nucl Med Biol 2005;32:719–25.

[21] Busk M, Jakobsen S, Horsman MR, Mortensen LS, Iversen AB, Overgaard J, et al. PET imaging of tumor hypoxia using ^{18}F-labeled pimonidazole. Acta Oncol 2013;52:1300–7.

[22] Wild D, Schmitt JS, Ginj M, Mäcke HR, Bernard BF, Krenning E, et al. DOTA-NOC, a high-affinity ligand of somatostatin receptor subtypes 2, 3 and 5 for labelling with various radiometals. Eur J Nucl Med Mol Imaging 2003; 30:1338–47.

[23] Miederer M, Seidl S, Buck A, Scheidhauer K, Wester HJ, Schwaiger M, et al. Correlation of immunohistopathological expression of somatostatin receptor 2 with standardised uptake values in ^{68}Ga-DOTATOC PET/CT. Eur J Nucl Med Mol Imaging 2009;36:48–52.

Supplementary material available online

Supplementary Appendix, Table I and Figures 1 and 2 available online at: http://informahealthcare.com/doi/abs/10.3109/0284186X.2014.925577